Molecular Dynamics Study of the Role of the Free Surface on Block Copolymer Thin Film Morphology and Alignment

Christopher Forrey,[†,*] Kevin G. Yager,[‡] and Samuel P. Broadaway[§]

[†]Center for Devices and Radiological Health, Food and Drug Administration, [‡]Center for Functional Nanomaterials, Brookhaven National Laboratory, and [§]Department of Mathematics and Computer Science, Wesleyan University

ABSTRACT Next-generation applications of block copolymer thin films will require a better understanding of the driving forces unique to thin film coatings, specifically those arising from the polymer—air interface. Previous modeling studies of film morphology have treated rigidly confined films, neglecting free surface considerations altogether. We report in this article the first systematic molecular dynamics investigation of block copolymer thin film ordering for unconfined films. We investigate the molecular basis of the formation of a number of experimentally relevant coating features, including surface islands and vertical lamellae. Surface islands are found to form in response to film incommensurability, whereas commensurability considerations are insufficient to explain vertical lamellar formation. Dynamics of lamellar formation presented herein demonstrate that vertical lamellar orientation is initiated in the surface regions of the film, most strikingly at the free surface. We conclude that the free surface plays a pivotal role in the free energy balance determining overall film morphology, and that confinement models provide an incomplete explanation of the physical basis of morphology selection in block copolymer coatings.

KEYWORDS: block copolymer · thin film morphology · lamellar alignment · molecular dynamics (MD) · simulation

As the scope of technology progresses to smaller and smaller length scales, block copolymers, well-known for the self-assembled nanoperiodic structures that arise during microphase separation,[1] offer a unique means to pattern and manipulate matter at the nanoscale. While block copolymers have been widely studied as pattern transfer masks for next generation lithography applications, a diverse set of novel applications have been proposed, including fuel cell membranes,[2] virus filtration membranes,[3] photonic band gap materials[4,5] and drug delivery vectors.[6]

Recently, drug-impregnated block copolymers have begun to be utilized as coatings for implantable devices, most notably coronary stents.[7−12] While the importance of morphology is clear for lithographic applications, it should be noted that successful development of block copolymer-based implantable coatings also requires a thorough understanding of and exploitation of nanoscale features. For example, morphology will dictate the pathway of drug through the coating, which in turn will affect the release rate of drugs. The coating surface itself is of great interest as it serves as the primary material/biology interface. Recent studies have demonstrated that block copolymer surface features can affect aspects of biological response *in vitro*, including protein adsorption,[13] cell adhesion[14,15] and differentiation.[16]

While a great deal is understood of block copolymer bulk behavior, one of the challenges to exploiting thin film morphologies will be to better understand the driving forces and additional morphological features unique to thin films. There are two important considerations introduced by the thin film geometry: the presence of interfaces with nonpolymeric phases and the limitation of a finite amount of material. Microphase separated structures associated with a directionality (lamellae and cylinders) can become oriented with respect to film interfaces under certain conditions. In most applications, one of the interfaces is a free interface, for which there is a difference in the surface tensions of the two blocks. Substrates also tend to favor one of the blocks over the other, as special treatment is required to achieve so-called "block-neutral" substrates. Consequently, interfaces are often preferentially wetted by one of the blocks, leading to the formation of lamellae oriented parallel the plane of the film, referred to as the horizontal lamellar (HL) orientation. When both interfaces are wetted by the same block, the film is said to display symmetric wetting, whereas when the interfaces are wetted by different blocks, the film is said to display asymmetric wetting. In cases where the net energetic preference of the substrate for a specific block is neutralized, lamellae oriented perpendicularly to

* Address correspondence to christopher.forrey@fda.hhs.gov.

Received for review December 16, 2010 and accepted February 14, 2011.

Published online March 11, 2011
10.1021/nn103502p

the film plane, known as vertical lamellae (VL), have been demonstrated to arise in certain situations. While vertical lamellar morphologies are highly desirable technologically, it is not fully understood why these structures form.

An additional well-known morphological feature unique to thin films is the formation of islands/holes at the free surface.[17] Islands form only on horizontal lamellar films, with the uppermost layer only partially completed, and are a consequence of the limitation to a finite amount of material. The resulting surface topography is quantized, with the film height profile characterized by step-like increments comparable to the interlamellar spacing, L_o.

Given the complexity of factors influencing morphology, studies of thin film physics have largely adopted a simplified approach in which the film is bounded by two parallel substrates.[18] While this confinement approach has provided a common and tractable system suitable to experiment,[19] theory,[20,21] and simulation,[22,23] it necessarily excludes the important consideration of the film free surface. Molecular dynamics and Monte Carlo studies, for example, have utilized purely repulsive force fields,[24−29] an approach that greatly reduces computational demand, yet is limited in scope to confined films.

The majority of block copolymer applications, on the other hand, call for coatings rather than confined films. Copolymer solutions are typically spin-cast onto the substrate (spray- and dip-coating are also common), resulting in unoriented and disordered (bicontinuous) structure. An ordered morphology, such as a cylinder or lamellar phase, develops upon annealing. In this contribution, we model this experimental procedure, using coarse-grained molecular dynamics simulation to investigate the process by which equilibrium structure arises for diblock copolymer thin film coatings. In addition, we seek to determine the degree to which insights obtained from confined film systems are suitable to nonconfined films.

RESULTS AND DISCUSSION

Our simulation model, detailed in the Methods section, is summarized in Figure 1 and described briefly here. Chains are composed of two chemically distinct blocks, type A (green) and type B (red) of equal length. Both blocks are composed of coarse-grained beads, for which nonbonded interactions are determined by pairwise Lennard-Jones potentials. Interactions are not truncated at the energy minimum, as for purely repulsive systems, but rather include an attractive tail at larger separations. Thus, polymer−polymer nonbonded interactions provide for

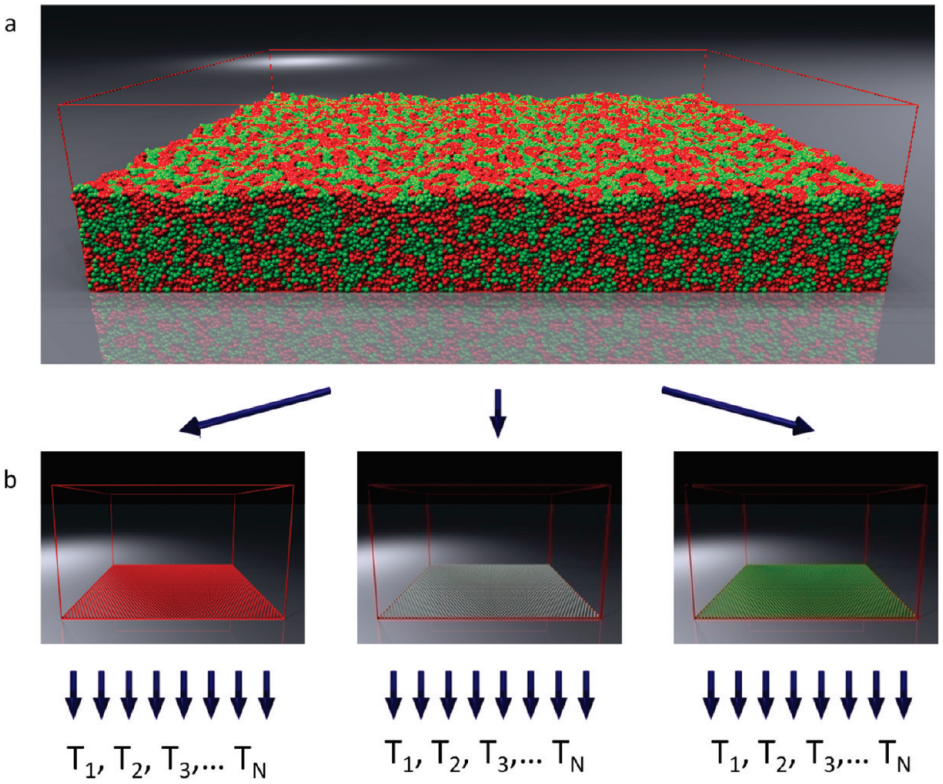

Figure 1. Simulation overview. (a) The starting point of each simulation run is a structure in which blocks are locally segregated but not globally aligned, preventing bias due to initial conditions. The simulation box is under-filled with beads, giving rise to polymer/air interface. (b) Substrate beads affixed on the lower box boundaries provide attractive interactions with polymer beads. The starting structure is placed on three-different substrate types, whose block-preference is color coded (gray = block-neutral) and further described in the text. For each substrate type, a series of independent heating (2 million steps) and annealing (12 million steps) simulations is performed, as signified by the series of vertical arrows below each substrate type.

film cohesion. The simulation box is under-filled, giving rise to a free polymer−air interface. Note that the polymer−air interface, at which polymer density decreases to zero, arises solely due to cohesive polymer interactions and does not require the use of solvent or "air" beads. The loss of polymer contacts at the polymer−air interface gives rise to a surface tension, the magnitude of which is dictated by bead cohesion strength. In the present work, type-A bead self-cohesion was parametrized to be stronger than type-B bead self-cohesion. Cross-type (type A/type B) cohesion was parametrized to be weaker than both A/A and B/B interactions. As detailed in the Supporting Information, an important criteria for our selection of nonbonded interaction parameters was to produce A- and B-blocks that are characterized by a difference in surface tension, $\Delta\gamma$, of about 7 mN/m. A non-negligible $\Delta\gamma$ is required to form morphological features unique to block-copolymer coatings, as will be seen presently. Relative bead cohesion strengths also determine the energetic mismatch parameter, χ. The product of χN, where N is the number of repeat units, describes the degree of block segregation, with microphase separation being predicted to occur at approximately $\chi = 10.5$. As detailed in the Supporting Information section, for our model, $58 < \chi N < 120$ over the range of conditions in this study, indicating that our model films are within the strong segregation limit.

The starting configuration in our simulations, with blocks locally segregated but not globally aligned, was chosen to mimic experiments utilizing spincast films and to ensure that final simulated morphologies are unbiased by initial configuration. The disordered starting structure was placed onto three substrate types, whose block preference is quantified by a Γ parameter (described in the Methods section): block-B-preferring ($\Gamma = 0.2$), block-A-preferring ($\Gamma = 0.8$), and block-neutral ($\Gamma = 0.50$). Films on each substrate type were subjected to a series of individual thermal treatments, each involving a two million step heating stage, starting at 23 °C and terminating at a unique annealing temperature, ranging from 107 to 309 °C. The annealing temperatures, once attained, were maintained for 12 million timesteps, and the structure and dynamics of film morphology were monitored continuously.

Experimentally, ordered film morphologies are attained by thermal annealing and are subsequently "locked in" by rapid cooling upon removal from an oven. The range of annealing temperatures employed in this study extends beyond those typical for experiments and therefore provides a breadth of temperature-based behavior that is helpful in discerning the physical basis of the complex morphological behavior observed in our model films. Our simulation model allows us to extend the annealing temperatures to high range for two reasons: (1) the simulation chain is not susceptible to chemical degradation at elevated temperatures; (2) the simulated chain is very strongly segregated at lower temperatures ($\chi N \approx 120$), allowing us annealing to higher temps while still remaining in the relevant temperature range below the order−disorder transition.

Neither block exhibited signs of order consistent with glassy or crystalline phases, with the exception of a slight periodicity in the density profile localized at the polymer−substrate interface. This local ordering, consistent with previous experimental measurements of polymer coatings,[30] does not persist for more than a few nm into the film structure and does not influence overall film morphology. Simulated film thickness is approximately 30 nm, with exact values varying slightly as a function of temperature, substrate type, morphological orientation, and presence or absence of surface islands.

Equilibrium Film Morphology and Dynamics of Lamellar Ordering as a Function of Substrate Type. We begin by considering simulations of lamellar ordering on each substrate type using a single thermal treatment, in which films were heated from 23 to 124 °C over 2 million steps and subsequently annealed at 124 °C for 12 million steps. Chronological snapshots of film morphology, along with the temperature profile, are shown in Figure 2.

Final morphologies (Figure 2, column D) can be classified based upon the orientation of the lamellae with respect to the substrate. Horizontal lamellae (HL) were formed on block-preferring substrates ($\Gamma = 0.2$ and $\Gamma = 0.8$), whereas a vertical lamellar (VL) structure was formed on the block-neutral substrate ($\Gamma = 0.5$). For the HL films, the identity of the substrate-wetting block was dictated by substrate block preference, whereas the lower surface tension block (type B, red) was found to wet the polymer−air interface regardless of the identity of the substrate-wetting block. Thus, films display both symmetric wetting ($\Gamma = 0.2$) and asymmetric wetting ($\Gamma = 0.8$). While the asymmetric film comprises fully completed layers, the symmetric film displays a surface island covering roughly half of the upper surface layer. Island formation is a consequence of film incommensurability, a condition in which the system lacks a precisely required number of chains per unit surface area to form a completed layer structure. The fact that our model can produce both completed-layer or surface island structure—depending on substrate block preference—is evidence of a significant $\Delta\gamma$. The influence of $\Delta\gamma$ results in the lower γ block wetting the free surface. For a negligible $\Delta\gamma$, HL film structure would simply invert based on substrate preference.

That equivalently parametrized chains can form both sysmmetric and asymmetric wetting films, depending on the substrate preference, indicates that both substrate and free surface preferences ($\Delta\gamma$) exert significant influence on lamellar morphology. The influence of $\Delta\gamma$ will be subsequently discussed when addressing the basis of VL formation, and island formation will be addressed in a subsequent section.

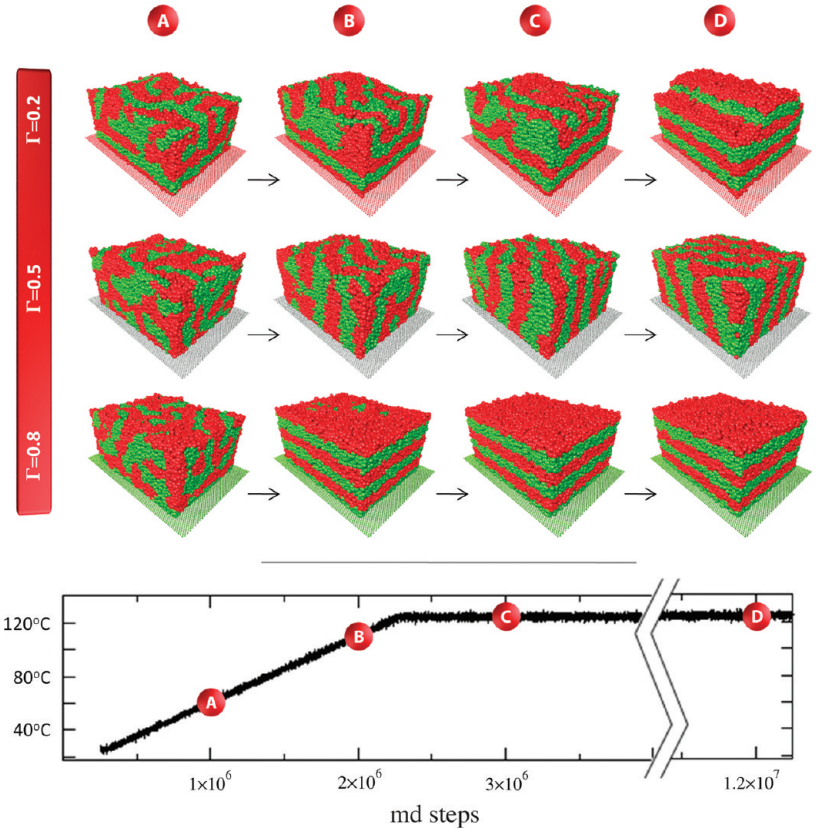

Figure 2. Time evolution of lamellar order on substrate types $\Gamma = 0.2$, $\Gamma = 0.50$, and $\Gamma = 0.8$ for a single thermal treatment. The thermal treatment profile is plotted at the bottom. On each row, sequential snapshots of film morphology are given, with substrate preference indicated by color (see perimeter of substrate beads beneath film structure) and Γ parameter. The time/temperature points for the snapshots are indicated by the symbols A, B, C, and D. The set of final structures (column D) display a number of experimentally observed features, including symmetric horizontal lamellar wetting and surface islands ($\Gamma = 0.2$), asymmetric horizontal lamellar wetting ($\Gamma = 0.8$), and vertical lamellar structures ($\Gamma = 0.5$, neutral substrate).

However, it should be pointed out now that the formation of a surface island on the $\Gamma = 0.2$ film does not imply that surface islands are characteristic of symmetric wetting films or that completed layer structures are characteristic of asymmetric films. Rather, the temperature and number of chains in the simulation box will also help determine which substrate preference gives rise to completed layers *versus* surface islands. However, the results at 124 °C do conform to the general expectation that, for a given film thickness, while a given film type (symmetric/asymmetric) forms completed layers, the opposing film type (asymmetric/symmetric) will form islands.

Remarkably, from consideration of a single annealing temperature, our approach has reproduced important experimentally observed morphological features of block copolymer thin film coatings. Molecular dynamics is a particularly powerful tool not only in its ability to predict film structure, but furthermore in providing great detail of the evolution of ordering. We now explore the time-evolution of the morphologies obtained at 124 °C. A rudimentary picture of ordering dynamics is provided in Figure 2, in which lamellar order can be seen to arise progressively with time on each substrate type. A more detailed picture of ordering dynamics is provided in the Supporting Information section in the form of a full movie of lamellar ordering on each substrate type, comprising 4000 individual frames covering 9 million molecular dynamics steps.

To follow the dynamics of lamellar alignment quantitatively, we define an order parameter, ϕ, which measures the average alignment of chain end-to-end vectors with the film normal:

$$\phi = \frac{1}{N}\sum_{i}^{N}\frac{\mathbf{R}_i}{|\mathbf{R}_i|}\hat{n} \qquad (1)$$

where N is the number of chains, i is the chain index, $\bar{\mathbf{R}}_i$ is the end-to-end vector of chain i, and $\hat{n}$ is the film normal (which is parallel to the z-axis in our model). By definition, $0 < \phi < 1$, with $\phi > 0.5$ corresponding to HL order and $\phi < 0.5$ corresponding to VL order. For the VL structure, ($\Gamma = 0.5$), we are interested in investigating where lamellar order is initiated within the film. To do so, four regions of the film are distinguished based on vertical position as illustrated in Figure 3a. As illustrated in Figure 3b, each film region is associated with a unique color scheme, to be used in plotting ϕ data: black, substrate proximal region; red, interior lower region; green, interior upper region; blue, free surface

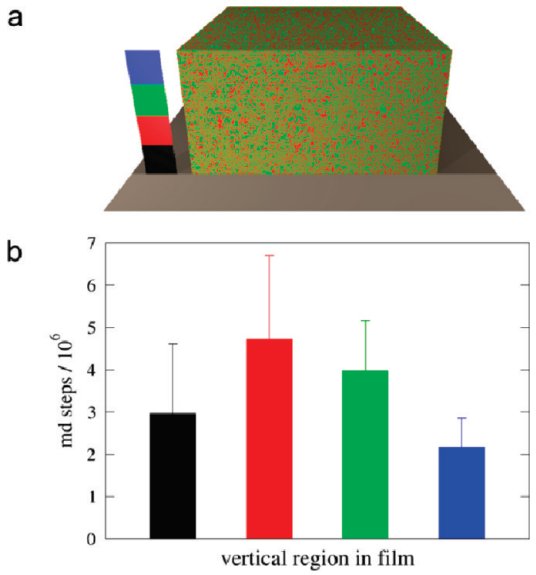

Figure 3. Appearance time of vertical lamellar order on block-neutral substrates as a function of vertical position in the film: (a) color coding of film region by vertical position; (b) the average number of timesteps required for vertical lamellar order to arise, on a block neutral substrate, is given for each region in the film.

proximal region. For films formed on each substrate type and for each time step, ϕ was calculated independently for each of the regions and the results were plotted in Figure 4.

On the basis of the quantitative information provided in Figure 4, as well as the observed film morphology in Figure 2, we can summarize the dynamics of lamellar ordering as follows. For block-preferring substrates, HL order is initiated by preferential block-wetting at the substrate interface and propagates continuously from the substrate interface with time. For the asymmetric film, a completed layer structure has formed after only 2 million steps (Figure 2, Figure 4c). For the symmetric film at this incommensurate thickness, propagation of lamellar order is considerably slower, with island formation requiring in excess of 8 million molecular dynamics steps (Figure 2, Figure 4a). The slower dynamics is evidence of an energy barrier corresponding to loss of neighbor contacts during island formation.

For the film on the block-neutral substrate, VL order is visible in both the substrate and free surface regions before arising in the film interior. VL ordering time, defined for each individual run as the initial time for which $\phi < 0.325$ (see dashed line in Figure 4b), has been averaged for simulations with annealing temperatures in the range 84 °C < T < 174 °C and plotted in Figure 3b. VL ordering in nonsurface regions is seen to lag behind VL ordering in the surface regions by as many as 2 million molecular dynamics steps.

Interestingly, regardless of substrate type, films display both blocks at the free surface for at least the first million simulation steps, indicating chain configurations favorable to VL order, as seen in Figure 2, column A.

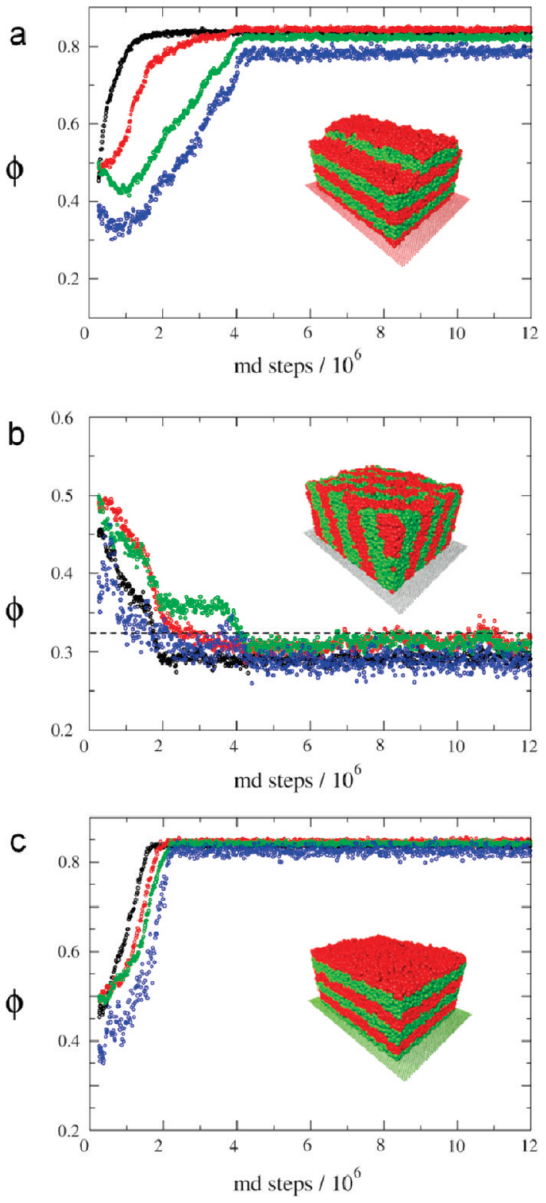

Figure 4. Time evolution of lammellar order and alignment: $\phi > 0.5$ indicates HL orientation, $\phi < 0.5$ indicates VL orientation, and $\phi = 0.5$ indicates lack of orientation. Colors correspond to different vertical positions in the film, as described in Figure 3a. Horizontal lamellar order can be seen to propagate progressively from the substrate (a,c), where surface/polymer interactions favor horizontal lamellar order. Vertical lamellar order clearly originates in the surface regions on block-neutral substrates.

Indeed, ϕ values in the free surface region in this early time frame are consistent with VL order. On block-preferring substrates, HL arises in the free surface region only after HL order has been established in the remainder of the film, as shown in Figure 4a,c.

Remarkably, results on the dynamics of lamellar ordering suggest that, on block-neutral substrates, VL order is preferred at both the free surface and substrate surface. Without substrate block preference, VL spreads from the surface regions to the film interior. However, surface preference for VL is

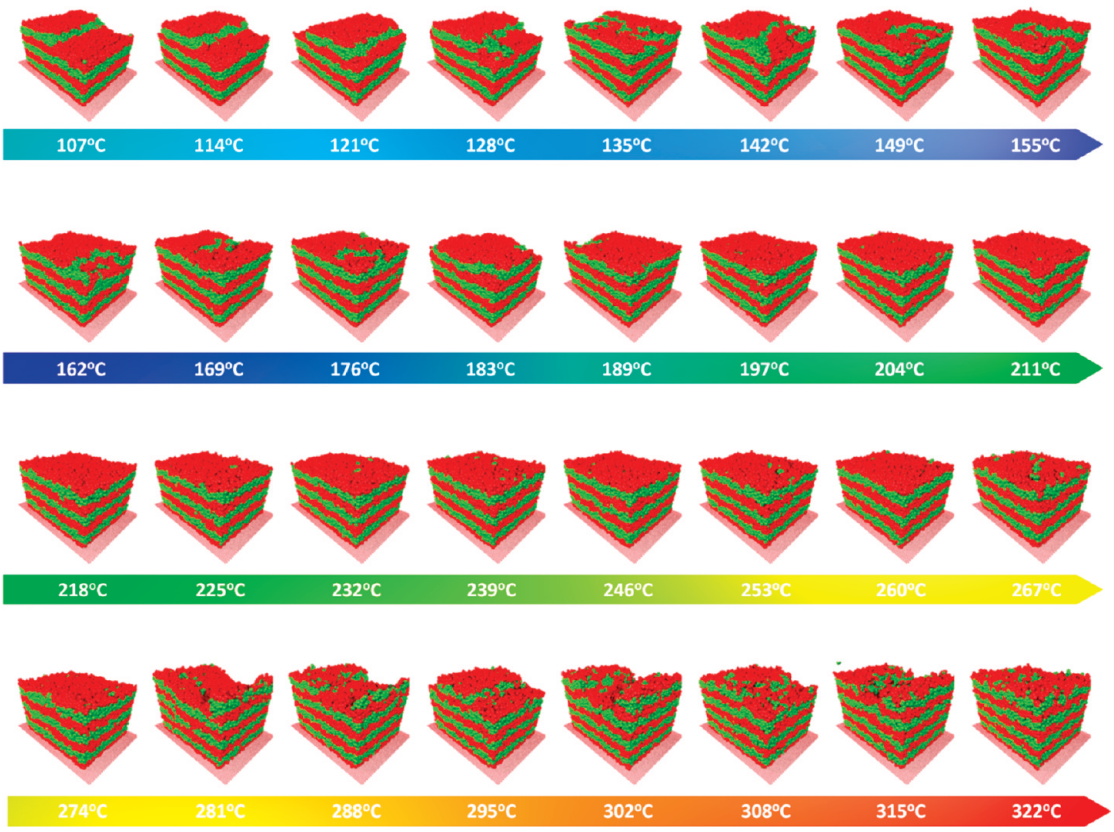

Figure 5. Final structures for films obtained on Γ = 0.2 substrate. Each snapshot in this series was obtained at the end of an independent heating/annealing simulation (see Figure 2 for a single temperature treatment), with the annealing temperature indicated beneath the film structure. Symmetric HL films are formed at all temperatures. At the lowest temperature, a partial surface lamellar layer is evident. As progressively higher annealing temperatures are considered, surface islands grow and eventually a complete upper layer is formed. More than a full cycle of this behavior is captured in the temperature range considered in this study.

eventually overtaken by HL order imposed by substrate preference.

Temperature Dependence of Film Morphology and the Role of Film Commensurability in VL Formation. Surface tension considerations in our model disfavor VL formation per unit area of free surface by about 3.5 J/m^2 (= $\Delta\gamma$/2). To understand the basis of VL formation, we must identify the free energy considerations that offset the surface tension penalty. Confinement studies have clearly established that film incommensurability can drive VL formation. Our simulated films are only a few lamellar repeats thick and thus are potentially strongly influenced by incommensurability. However, film morphologies presented in Figure 2 represent evidence that VL formation is not due solely to incommensurability. To see that this is the case, consider that HL and VL structures compete for selection under a given set of conditions. The asymmetric HL structure from the Γ = 0.8 substrate, being constituted of completed lamellar layers, likely represents a near-commensurate structure, yet the VL structure was selected on the block-neutral substrate. This suggests that VL morphology does not arise simply to alleviate film incommensurability. However, to draw conclusions about the role of commensurability in VL formation, we would need to know with certainty that the asymmetric structure is commensurate. While the structure on the Γ = 0.8 substrate is composed of completed layers, this alone is not proof of commensurability, as chains may have undergone some degree of stretching or contortion to avoid island formation. For this reason, we cannot know for certain that completed-layer structures formed at 124 °C, or at any single temperature, are commensurate. However, by considering a set of final film structures formed using a wide range of finely spaced annealing temperatures, we assume that the resulting set of film structures will contain at least one nearly commensurate structure.

In Figure 5 and Figure 6, equilibrium film morphologies are presented on block-preferring substrates. Snapshots are shown of the final HL structures obtained on Γ0.2 and Γ0.8 substrates over a series of annealing temperatures ranging from 107 to 322 °C. (Structures shown represent a subset of a larger set of simulations performed, with annealing temperatures spaced by 3.5 °C.) Each structure was obtained at the conclusion of an independent simulation, similar to the simulations shown in Figure 2. A revealing trend can be discerned, the cycling of morphological behavior with increasing temperature; the initiation of surface islands

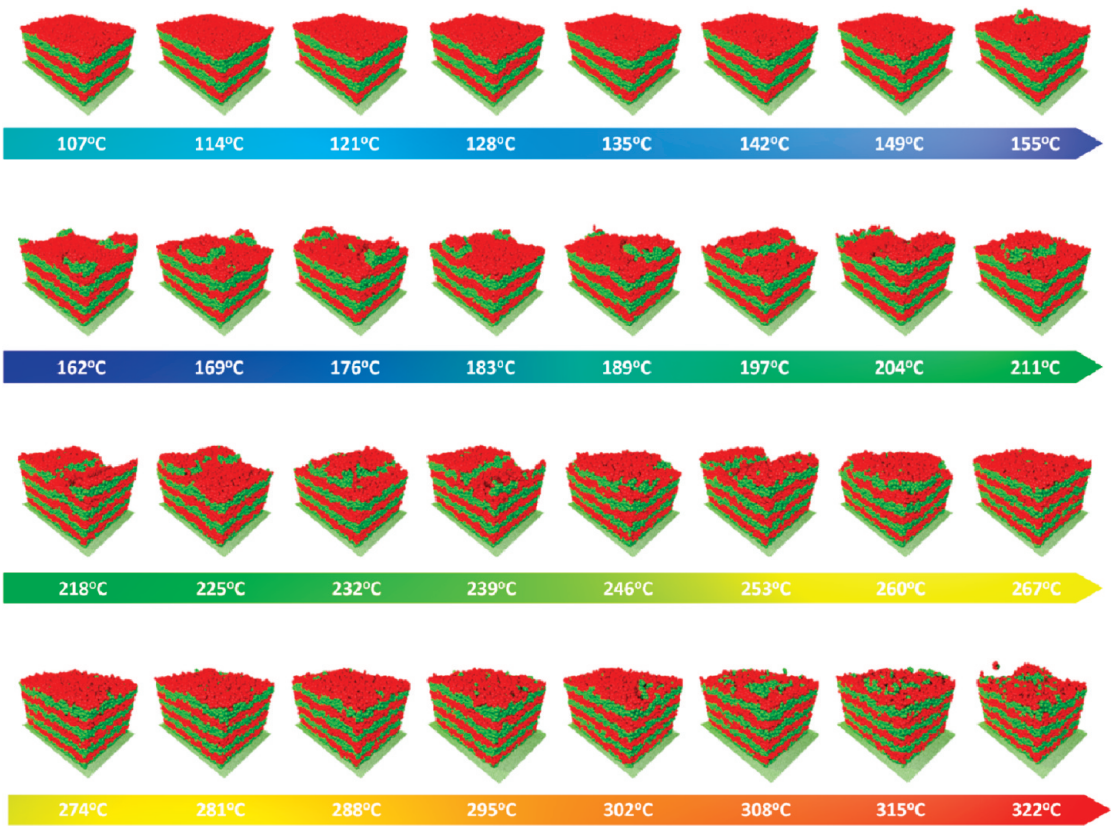

Figure 6. Final structures for films obtained by thermal treatment on $\Gamma = 0.8$, substrate. Asymmetric HL films are formed at all annealing temperatures. As was the case on the $\Gamma 0.2$ substrates (Figure 5), island formation/layer completion with increasing temperature is observed.

at the free surface is followed by progressive island growth, leading to a partial layer structure with a surface "hole". Upon layer completion, a near-commensurate completed layer structure persists over a range of temperature before the cycle is repeated. At least one full cycle of layer initiation/completion occurs within the simulation temperature range for both the symmetric and asymmetric films. The consistency of the island growth/completion trend with temperature indicates that the final structures obtained at the conclusion of each annealing stage have attained equilibrium. We note that the present study is the first molecular dynamics study to observe surface island formation.

In contrast to the temperature-driven cycling of HL morphological features on block-preferential substrates, we find that VL form on block-neutral substrates regardless of annealing temperature. As we have explored annealing temperatures spanning more than a full cycle of HL island formation and completion, at least two near-commensurate structures must fall within this range, one symmetric structure and one asymmetric structure. Were VL attributable solely to incommensurability, we should have observed at least two HL structures among the full set of structures over all annealing temperatures. We conclude that VL are lower free energy structures, regardless of the commensurability state of alternative HL structures.

In seeking to understand the overall free energy balance favoring VL formation over HL formation on block-neutral substrates, it is of interest to compare the energies of the HL and VL states. To facilitate this comparison, HL films (both symmetric and asymmetric) formed on block-preferring substrates were transferred to block−neutral substrates, and the energy of the resulting set of HL and VL structures were then measured. As the substrate was set to block-neutral, energy differences can be attributed to internal film energy. We emphasize that such "transplanted" HL structures are not the equilibrium structures on block-neutral substrates, but nonetheless allow for a direct comparison of the internal energy of the set of candidate HL and VL films as they would appear on block-neutral substrates.

In Figure 7, the energy of HL and VL films on block-neutral substrates is plotted as a function of annealing temperature. Remarkably, the VL structures are observed to be of higher energy than HL structures at every temperature. The finding that HL films spanning the full cycle of commensurability are lower energy than VL films further confirms that VL do not arise simply as a lower energy alternative to incommensurate HL structures.

Surface Configurational Entropy and VL Formation. We have thus far demonstrated that VL films are higher

energy than corresponding HL structures and yet are selected as equilibrium structures on block-neutral substrates. For this to be the case, entropy must favor VL formation. We now investigate the role of one possible entropic contribution favoring VL formation. It has been argued that polymer chains in the vicinity of a hard wall are subject to a localized surface entropy field that drives the chains to orient with the chain axis in the plane of the surface,[20,31,32] which in block-copolymer lamellae is the chain orientation for VL alignment. We have shown that VL formation is surface initiated.

We now seek an estimate of the degree to which the surface entropy field drives this surface initiated VL formation. The signature of the surface entropy field is the local extension of polymer configurations parallel to a flat impenetrable barrier, as illustrated on the left-hand side of Figure 8. The altered end-to-end separation distributions translate directly to an increase in the entropic force required to extend the chains perpendicular to the wall. Figure 8 further illustrates the change in surface-local chain configurations in going from surface-entropy-aligned to HL-aligned morphologies. The work done against the surface entropy field, W_S, should disfavor HL formation and it would be of interest to compare its magnitude with the surface energy penalty to form VL. W_S can be determined from knowledge of the number of chains (N_S) in the near surface region (we will treat the substrate and free surfaces independently), the difference in the average vertical extension (ΔR_z) of chains in the surface region of a HL film compared to that of a surface-entropy-aligned film, and the entropic force resisting such perpendicular elongation normal to the surface (f_z):

$$W_S = N_S \times f_z \times \Delta R_z \quad (2)$$

A challenge is presented in determining the surface-entropy-aligned chain configurations. For homopolymers, any surface-localized chain extension can be attributed unambiguously to the surface entropy field. For block copolymers, the surface entropy field cannot be determined from chain configurations, as numerous other factors influence chain alignment, including $\Delta\gamma$ and substrate block-preference. To isolate localized chain alignment effects due to surface entropy, a homopolymer model—with average chain extension matching that of the block copolymer chains—was utilized and is described further in the Methods section. In Figure 9, the components of chain end-to-end separation are plotted as a function of vertical distance from the substrate for the homopolymer model. Chain flattening is evident near both substrate and free surfaces and is used to define the surface regions (darkened area). End-to-end separation profiles were determined for substrate, bulk, and free surface regions and are plotted at the bottom of Figure 9. The substrate and free surfaces are seen to affect the chain

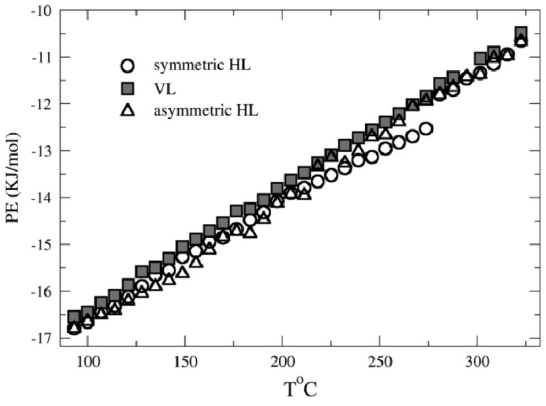

Figure 7. Internal energy as a function of lamellar orientation and temperature. Horizontal lamellar (HL) film morphologies formed on block-preferring substrates (see Figure 5 and Figure 6) were resituated on block-neutral substrates, allowing a direct comparison of HL and VL film energies on neutral substrates. VL structures are seen to have higher energy than both the symmetric and asymmetric HL structures over the full range of annealing temperatures considered in the study.

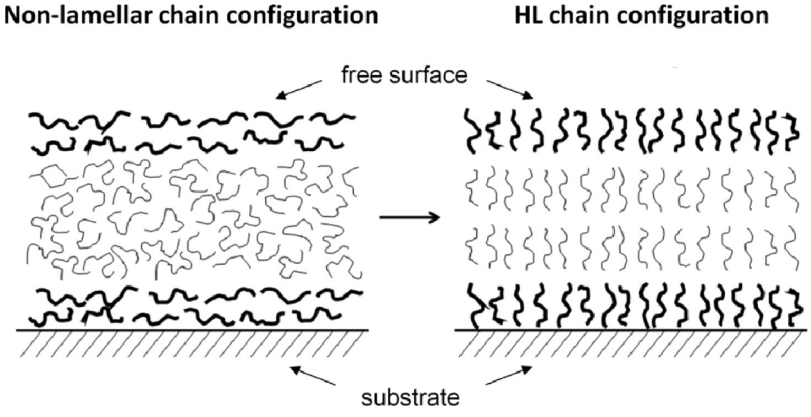

Figure 8. Schematic illustration of surface-entropy-aligned *vs* HL-aligned chain configurations in surface regions. Chains align parallel to the substrate and free surfaces due to the surface entropy effect (illustration, left), giving rise to large forces to extend/align chains perpendicular to the surface. HL morphologies require vertical chain alignment (illustration, right). By determining the difference in perpendicular extension from the surface-entropy-aligned configurations to the HL configurations in the surface region, an estimate of the free energy penalty of HL formation is determined (see text).

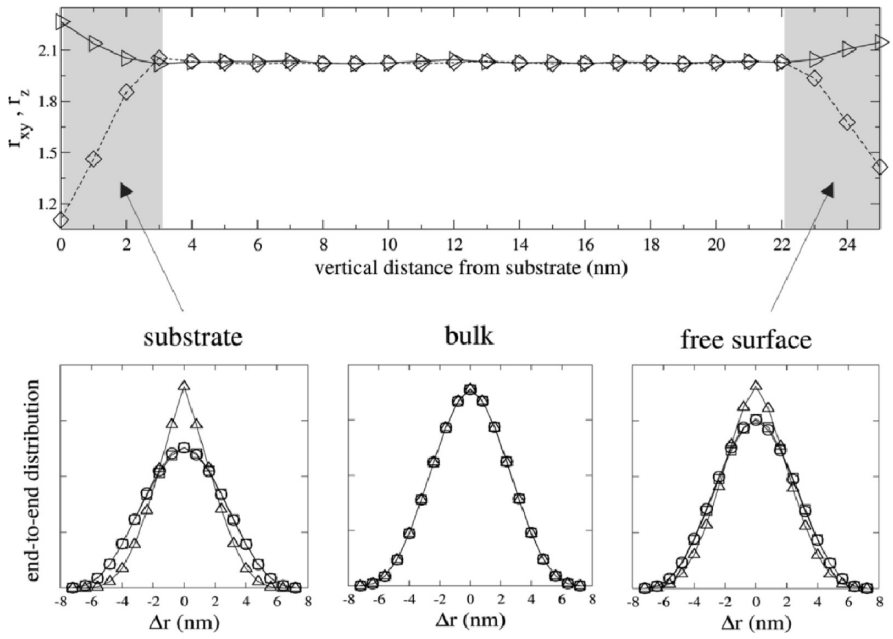

Figure 9. Surface entropy induced localized chain alignment. Top: Surface localized chain flattening is evident in average end-to-end extension profiles. Bottom: Distribution of end-to-end separations is plotted for substrate, bulk, and free surface regions. Data for the *z*-component of the end-to-end distance is shown using triangles. In the upper section, data for the *xy* plane is shown using diamonds, whereas the *x*- and *y*-dimensions are shown in the lower section using circles and squares, respectively.

TABLE 1. Surface Entropy Field Free Energy Terms

	substrate			free surface		
temp (°C)	*N*	f_z (pN)	ΔR_z (nm)	*N*	f_z (pN)	ΔR_z (nm)
85	697	0.95	2.11	744	0.72	1.98
144	652	1.12	1.97	760	0.75	1.79
204	602	1.19	1.81	798	0.89	1.60
263	552	1.29	1.64	666	0.93	1.45

dimensions primarily by reducing the *z*-component of the end-to-end distance, whereas the increase in-plane (*xy*) chain extension is relatively small, in agreement with experimental studies of chain configurations in ultrathin films.[33] Extension forces perpendicular to each surface are determined as described by Sommer *et al.*[31] *N*, f_z, and ΔR_z for the substrate and surface regions are given in Table 1 for four temperatures: 85, 144, 204, and 263 °C.

The work done against the surface entropy field to form HL is plotted per unit surface area for both the substrate and free surface regions in Figure 10. The straight lines are linear fits to the data. By considering the work per unit area, the surface configurational entropy effect can be directly compared with the block surface tension difference, $\Delta\gamma$. Values for the substrate−polymer interface fall between 0.7 and 0.9 mN/m, whereas values for the free surface range from 0.5 to 0.7 mN/m. The relatively modest surface configurational entropy values can reasonably be expected to drive VL at the substrate, where there is no energy penalty to VL formation. For systems with particularly

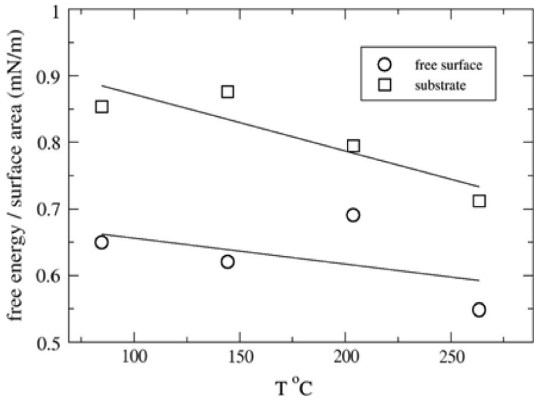

Figure 10. Work done against surface entropy field per unit surface area. Free energy per unit surface area required to align surface−proximal chains such that chains are vertically aligned, consistent with HL structure. While this entropic free energy cost disfavors the HL orientation, it is smaller than the surface tension penalty of forming VL, $\Delta\gamma/2-3.5$ mN/m.

small $\Delta\gamma$, PS/PVME for example, we would also expect surface configurational entropy to drive VL formation. At the free surface, on the other hand, the surface entropy work is insufficient to tip the free energy balance in favor of VL. Nonetheless, our simulated morphologies indicate that VL is most strongly favored at the free surface. Previous theoretical work based on confined films has predicted that VL can be attributed to incommensurability or surface configurational entropy considerations. Our simulations of free surface coatings indicate that these considerations contribute to VL formation, but are insufficient to explain the role of the free surface

in initiating VL order. We suggest that there is an additional entropic consideration due to interfacial fluctuations that drives VL formation at the free surface. We will explore this possibility in a future study.

Horizontal Lamellar Film Morphology. We now explore the physical origin of surface island formation, which we argue can be suitably explained by molecular-level commensurability arguments. At any given temperature, a film will seek to form a structure comprising completed layers (to avoid loss of neighbor contacts) while maintaining bulk-like chain stretching. Confinement studies allow the systematic investigation of incommensurability in response to imposed film height, as chains are forced to stretch or contract along the lamellar normal in order to accommodate an integer number of lamellae between the plates. While film height is unconstrained for free surface films, incommensurability can arise due to lateral constraint. As temperature is increased, entropy-driven reduction in chain stretching can result in an incommensurate structure, as we now discuss.

Consider the morphological behavior of the asymmetric films with increasing temperature in Figure 6. At the lowest temperature shown, T = 107 °C, the film is composed of a near-commensurate completed layer structure. As temperature is increased, in order to maintain horizontal lamellae, films must either pay an island formation energy penalty or suffer an entropic penalty due to incommensurate chain stretching. Completed layer structures are sustained until about 155 °C, indicating that the film can withstand a certain degree of incommensurability *via* chain deformation. At higher temperatures, the entropic penalty becomes unsustainable and chains are ejected to the free surface, where they aggregate as islands. In this way, the free surface serves as an important outlet for internal frustration, allowing underlying chains to maintain bulk-like configurations. Further increase in temperature leads to the progressive growth and eventual completion of the partial layer structure, at which point the process begins anew. A similar trend is seen for the symmetric film in Figure 5.

A simplistic picture of this molecular interpretation is presented schematically in Figure 11a. At lower temperatures, chain extension normal to the lamellar repeat defines a characteristic lamellar spacing, L_o. As temperature is increased, axial stretching of chains is decreased. At higher temperatures, axial contraction is compensated for by lateral expansion, which in combination with lateral confinement leads to rearrangement into a film with more layers and a smaller L_o. As the film cannot expand in-plane, lateral chain expansion leads to chains being expelled to the free surface to form islands. In temperature regions where the film can form complete layers, the chain stretching free energy penalty is less than that for island formation. This molecular interpretation of HL film morphology is supported by the end-to-end distance behavior of block copolymer chains as a function of temperature, which is plotted in Figure 11b. Solid diamond data correspond to values obtained from the symmetric film, including structures shown in Figure 5. Open circle data corresponds to bulk simulations performed using the same chain parametrization as in the films. Temperature is plotted in reduced units, with reduced temperature, T^* = T/25 °C. The end-to-end distance of the bulk chains can be seen to decrease monotonically as temperature is increased. For the symmetric films, the end-to-end distance behavior follows that of the bulk material up to about 200 °C (T^* = 1.54), consistent with the temperature range over which surface islands are visible in Figure 5. This is evidence that surface islands provide a means for incommensurate films to relieve entropic frustration and re-establish bulk-like chain configurations. From 200 to 270 °C (T^* = 1.54−1.80); that is, for the near-commensurate asymmetric HL structure region, end-to-end distance is seen to increase with increasing temperature, as the laterally constrained chains are forced to accommodate thermal expansion parallel to the lamellar normal. The breadth of the completed layer temperature range and the nonmonotonic end-to-end distance behavior indicate that individual chains can stretch significantly to avoid the island formation penalty. In general, flexible chains can be expected to favor completed layers, whereas more rigid chains should be more susceptible to island formation or mixed morphologies.

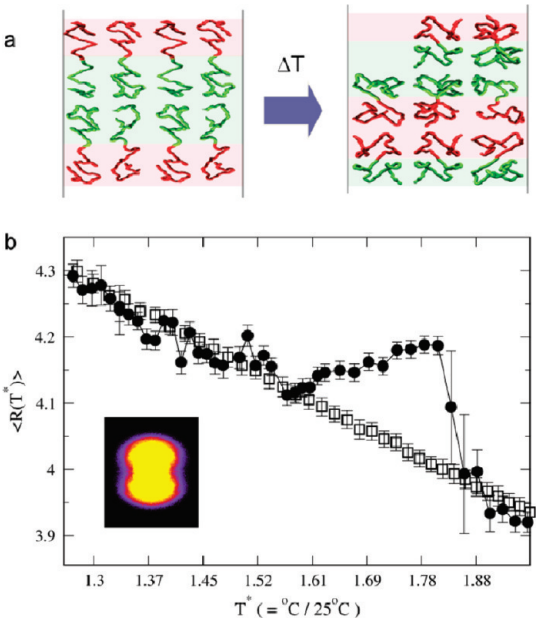

Figure 11. Chain extension and film commensurability in a HL film: (a) schematic illustration of chain configuration as a function of temperature; (b) average chain end-to-end distance for symmetric films formed on Γ0.2 (see Figure 5) and for bulk material.

We note that fixed in-plane box boundaries are essential to our commensurability-based interpretation of temperature dependent island formation for free

surface films. By making lateral box dimensions independent of temperature, we have assumed negligible lateral thermal expansion of our thin films. However, limited lateral mobility is likely a factor for experimental systems as well due to the slow dynamics of polymer chains[34] in relation to macroscopic in-plane film dimensions. In fact, the very presence of surface islands suggests constrained lateral motions; given sufficient freedom of lateral motion, films could simply rearrange to form completed-layer structures. We conclude that island formation arises as a result of film incommensurability, which is itself predicated on limited in-plane chain mobility.

While our simulations provide molecular-level insight into island formation, it should be noted that simulated surface islands differ from those observed experimentally in a subtle but significant way. In our system, the macroscopic film is modeled by applying a periodic boundary to the in-plane dimensions. Simulated surface islands are thus periodic, whereas experimentally observed islands appear without periods. Because simulated island structures are unable to aggregate with their periodic images, our simulation model thus introduces a free energy penalty to island formation that is somewhat larger than it would be for a macroscopic film. The effect of this energy penalty will be largest at the initial stage of island formation and will be mitigated in the latter stages, when the partial layer spans one of the box dimensions, reducing the periodicity to a single dimension. We do not expect that this free energy penalty should qualitatively affect the previously described chain entropy mechanism of island formation; the island formation penalty likely simply shifts the initial appearance of surface islands to slightly higher temperatures than would be the case for a truly macroscopic nonperiodic system. Furthermore, a free energy penalty resisting island aggregation is to some extent appropriate, as experiments have clearly demonstrated that surface islands do not aggregate without limit, but rather are characterized by a length scale at which island-size saturates[35,36] due to polymer fluctuations and to surface elasticity.

CONCLUSIONS

Using molecular dynamics, we studied the complex morphological behavior that arises on free-surface-containing symmetric diblock copolymer thin films as a function of temperature and substrate block-preference. We followed the dynamics of lamellar formation and presented evidence that vertical lamellar alignment is initiated at both of the surface regions. Surprisingly, vertical alignment was found to arise most rapidly in the free surface region, despite being disfavored by surface tension considerations.

Horizontal lamellar structures formed at increasing annealing temperatures displayed a well-behaved cycling of layer initiation, growth, and completion. By analyzing this behavior, it was demonstrated that island formation provides the film with an alternative to the excess (relative to bulk) chain stretching associated with incommensurate film structures.

Although horizontal lamellar structures were observed to be lower energy structures, vertical lamellar structures were observed to form on block-neutral substrates at every temperature considered. We report evidence that incommensurability alone is insufficient to explain VL formation and quantify the contribution due to surface local chain stretching.

We conclude that the free surface serves as an outlet for internal frustration, thus stabilizing horizontal lamellar alignment, while at the same time serving as the primary location of initiation of vertical lamellar order. Our results indicate that a better understanding of the complex free energy balance between horizontal and vertical lamellar morphologies of free surface films will require continued investigation of the role of the influence of the free surface on film morphology.

METHODS

Simulation Model. *Block Copolymers.* Block copolymers were modeled as linear chains of 10 coarse-grained beads, with each chain comprising a five-bead A-block and five-bead B-block. Individual beads represent aggregate behavior of a grouping of chemical atoms or repeat units, allowing computational resources to be expended on larger system size and longer time scales, both of which are essential for studying lamellar formation in block copolymer films. As we are interested in exploring fundamental (rather than block-specific) driving forces of film morphology, we have not parametrized chains to model a specific block copolymer. To maintain generality, we have devised a generic block copolymer model to meet the following requirements: First, the block copolymer interactions must be such that the strong segregation limit applies. Second, the blocks must be characterized by a non-negligible difference in free surface tension, $\Delta\gamma$. Third, substrate−polymer interactions must be sufficiently strong to adhere the film to the substrate irreversibly. Fourth, the substrate block preference must ensure the wetting of the preferred block, which must be assignable as an input parameter.

To satisfy these criteria, the following set of potentials were utilized:

Pairwise consecutive beads along the chain are subject to a harmonic bond stretching potential,

$$U_{\text{bond}} = K_{\text{stretch}}(l - l_o)^2 \quad (3)$$

which maintains the separation distance of consecutive beads along the chain near the equilibrium bond length l_o. The bending energy potential for block copolymer chains is given by

$$U_{\text{bend}} = K_{\text{bend}}(\theta - \theta_o)^2 \quad (4)$$

where θ is the angle defined by a pair of consecutive bonds along the chain backbone. The angular potential serves to restore θ to an equilibrium value, θ_o, and is contributes to the overall stiffness of simulated chains. Nonbonded interactions

were modeled using Lennard-Jones potentials including an attractive tail between all bead types in our model:

$$U_{LJ} = 4\varepsilon\left[\left(\frac{\sigma}{r}\right)^{12} - \left(\frac{\sigma}{r}\right)^{6}\right] \quad (5)$$

Beads separated by less than $2^{1/6}\sigma$ experience a sharp r^{-12} repulsive potential, whereas bead pairs separated by more than $2^{1/6}\sigma$ experience a gradually decaying r^{-6} attractive potential. To ensure that interbead interactions include a sufficient portion of the attractive tail to ensure bead cohesion, a cutoff distance of 3σ was applied.

Block copolymer bead parameters are provided in Table 2. The difference in Lennard-Jones energy parameters between the two blocks satisfies two essential modeling goals: (1) An energetic mismatch parameter, χ, arises from bead parametrization and provides the driving force for microphase separation. As detailed in the Supporting Information section, χN values were determined for our model system at temperatures ranging from 85 to 323 °C. Values ranged from approximately 60 to 120, consistent with the strong segregation limit. (2) The difference in cohesive self-interactions of the two blocks gives rise to a difference in surface energy of the blocks, $\Delta\gamma$, of approximately 7 mN/m from 85 to 323 °C, providing the driving force for wetting of the free surface by the lower surface energy block-B. Details of the $\Delta\gamma$ determination are provided in the Supporting Information section.

Homopolymer. A homopolymer model film was employed to measure the surface entropy effect on local chain configurations at the substrate and free surfaces. Average chain extension in the homopolymer film should match that of the block copolymer film as closely as possible to ensure that the action of the surface entropy field on the homopolymer model serves as a suitable surrogate for the block copolymer film. Parameter values used were identical to those for block copolymer beads, with the exception of k_{bend} and $\varepsilon_{homopolymer}$, as indicated in Table 2. Lennard-Jones parameters were selected such that $\varepsilon_{homopolymer} = (\varepsilon_A + \varepsilon_B)/2$, so that homopolymer beads have cohesive forces intermediate between type A- and B- self-interactions of the copolymer. Simulations of the homopolymer film using various k_{bend} values were performed to determine the value of the bending energy coefficient giving the same end-to-end distance found in the block copolymer film over the temperature range of interest in this study. Five values of k_{bend} were tested at four different temperatures: 85, 144, 204, and 263 °C. For each combination of k_{bend} and temperature, a simulation of 1 million molecular dynamics steps (NVT ensemble) was performed, with the average end-to-end distance being determined over the final 10 000 steps. $k^*_{bend} = 33$ meV/radian^2 was found to produce the same average chain extension as in the block copolymer film. As expected, a larger value of k_{bend} is required for the homopolymers to achieve the same average extension as the block copolymers, as block copolymers are subject to additional enthalpic stretching due to interblock repulsion. Chain configurations presented in Figure 9 were determined from the k^*_{bend} film.

TABLE 2. Polymer Chain Parameterization[a]

type	parameter	value
bond stretching	l_o (nm)	1.0
	$k_{stretch}$ (meV/nm^2)	12 800
bending	θ	180°
	k_{bend} (meV/radian^2)	0
		33.3[b]
Lennard-Jones	ε_{AA} (meV)	49.0
	ε_{AB} (meV)	25.8
	ε_{BB} (meV)	41.3
	$\varepsilon_{homopolymer}$ (meV)	45.2[b]
	σ (nm)	0.84
	σ_{cut} (nm)	2.5

[a] l_o, k_s, θ_0, σ, σ_{cut} homopolymer + block copolymer. [b] Unique to homopolymer.

TABLE 3. Surface/Polymer Interaction Parametrization[a]

$\Gamma = \varepsilon_{SA}/(\varepsilon_{SA} + \varepsilon_{SB})$	ε_{SA} (meV)	ε_{SB} (meV)
0.2	12.8	51.2
0.50	32.0	32.0
0.8	51.2	12.8

[a] $\sigma_{substrate}$ (nm) = 0.11.

Substrate. The substrate was modeled as a reflective boundary (lower z box boundary) affixed with a hexagonally patterned array of small radius ($\sigma = 0.112$ nm) Lennard-Jones beads (see Figure 1). The beads were immobilized and provided tunable attractive interactions with beads of type A and B, as defined by the Lennard-Jones energy parameters ε_{sa} and ε_{sb}. A convenient parameter is defined to describe the relative preference of the substrate for polymer beads, $\Gamma = \varepsilon_{sa}/(\varepsilon_{sa} + \varepsilon_{sb})$. In this study, we examine three different Γ values: $\Gamma = 0.2$, B-block favored by substrate; $\Gamma = 0.5$, no preference of substrate for either block; and $\Gamma = 0.8$, A-block preferred by substrate. Γ values and corresponding ε_{sa} and ε_{sb} values are given in Table 3.

Simulation Procedure. Molecular dynamics simulations were carried out using the LAMMPS simulation package made available by Sandia National Laboratories. Simulations of film ordering were performed using the canonical (NVT) ensemble and a time step of 1.74 ps. The simulated film systems included 52800 polymer beads and 3960 substrate beads in a simulation box of dimensions 45.7 nm × 36 nm × 51 nm. Periodic boundary conditions were applied in the xy plane, that is, in the plane of the film. The initial "spincast" structure was copied and used as the starting structure for simulations on each substrate type. Individual runs involved a 2 million step heating stage, in which the temperature was linearly ramped from 25 °C to a unique final annealing temperature, succeeded by a 12 million step annealing stage. Prior to the heating stage, a brief 10000 step Langevin dynamics run was performed using a unique random seed to give subsequent simulations a unique phase space trajectory.

Two nonfilm systems were used in this study: bulk simulations and simulations to determine χ. As opposed to our film systems, these systems do not require a polymer−air interface. Constant pressure and temperature (NPT) ensemble simulations were performed using a simulation box periodic in all three dimensions until zero pressure was established in all three dimensions, thus allowing the system to select its equilibrium density. Lamellar structures were used as initial configurations for bulk simulations. For χ determination runs at each temperature, three simulations were performed: one each for the pure components (homopolymer A and homopolymer B) and one for the mixture (block copolymers). Starting structures were randomly aligned. For both bulk simulations and χ determination simulations, after pressure equilibration, data collection was performed using the NVT ensemble, as detailed in the Supporting Information section.Periodic Box Size. For simulation runs involving film structure, periodic boundary conditions were used in the xy plane. Care must be taken to avoid finite box size artifacts related to the lamellar repeat length, L_o. For VL structures, the repeat length L_o is in the $x-y$ plane. Box sizes comparable to L_o may lead to nonphysical stresses, as chains would be required to undergo artifactual contortions in order to squeeze an integer number of L_o repeats into the periodic box. For box sizes much larger than L_o, on the other hand, the film does not "see" the periodic boundary, in that the film is free to choose the orientation and spacing of its lamellar repeat without the periodic box affecting the free energy of the film. We find that VL are formed spontaneously on block-neutral substrates, clearly demonstrating that lamellar orientation is insensitive to box dimensions for the selected box size.

Acknowledgment. We thank the Division of Electrical and Software Engineering (FDA) for use of the high performance computing facilities and the Division of Imaging and Applied Mathematics (FDA) for computational time. We also thank A. Bosse (NIST) and D. Saylor (FDA) for providing insightful comments. Research carried out in part at the Center for Functional

Nanomaterials, Brookhaven National Laboratory, which is supported by the U.S. Department of Energy, Office of Basic Energy Sciences, under Contract No. DE-AC02-98CH10886.

Supporting Information Available: Additional detail on preparation of starting structure, determination of χ, and determination of surface tension, γ. Movies of the starting structure and lamellar ordering process are also provided. This material is available free of charge *via* the Internet at http://pubs.acs.org.

REFERENCES AND NOTES

1. Hamley, I. W. *The Physics of Block Copolymers*; Oxford University Press: UK, 1999.
2. Meier-Haack, J.; Taeger, A.; Vogel, C.; Schlenstedt, K.; Lenk, W.; Lehmann, D. Membranes from Sulfonated Block Copolymers for Use in Fuel Cells. *Sep. Purif. Technol.* **2005,** *41*, 207–220.
3. Yang, S. Y.; Ryu, I.; Kim, H. Y.; Kim, J. K.; Jang, S. K.; Russell, T. P. Nanoporous Membranes With Ultrahigh Selectivity and Flux for the Filtration of Viruses. *Adv. Mater.* **2006,** *18*, 709–712.
4. Kang, C.; Kim, E.; Baek, H.; Hwang, K.; Kwak, D.; Kang, Y.; Thomas, E. L. Full Color Stop Bands in Hybrid Organic/Inorganic Block Copolymer Photonic Gels by Swelling−Freezing. *J. Am. Chem. Soc.* **2009,** *131*, 7538–7539.
5. Kang, Y.; Walish, J. J.; Gorishnyy, T.; Thomas, E. L. Broad-Wavelength-Range Chemically Tunable Block-Copolymer Photonic Gels. *Nat. Mater.* **2007,** *6*, 957–960.
6. Guo, X. D.; Tan, J. P. K.; Kim, S. H.; Zhang, L. J.; Zhang, Y.; Hedrick, J. L.; Yang, Y. Y.; Qian, Y. Computational Studies on Self-Assembled Paclitaxel Structures: Templates for Hierarchical Block Copolymer Assemblies and Sustained Drug Release. *Biomaterials* **2009,** *30*, 6556–6563.
7. Kim, C. S.; Saylor, D. M.; McDermott, M. K.; Patwardhan, D. V.; Warren, J. A. Modeling Solvent Evaporation During the Manufacture of Controlled Drug-Release Coatings and the Impact on Release Kinetics. *J. Biomed. Mater. Res., Part B* **2009,** *90B*, 688–699.
8. McDermott, M. K.; Saylor, D. M.; Casas, R.; Dair, B. J.; Guo, J.; Kim, C. S.; Mahoney, C. M.; Ng, K.; Pollack, S. K.; Patwardhan, D. V.; *et al*. Microstructure and Elution of Tetracycline from Block Copolymer Coatings. *J. Pharm. Sci. 99*, 2777-2785.
9. Cho, J. C.; Cheng, G. L.; Feng, D. S.; Faust, R.; Richard, R.; Schwarz, M.; Chan, K.; Boden, M. Synthesis, Characterization, Properties, and Drug Release of Poly(alkyl methacrylate-*b*-isobutylene-*b*-alkyl methacrylate). *Biomacromolecules* **2006,** *7*, 2997–3007.
10. Gu, X. Z.; Kuang, Y. B.; Guo, X. X.; Fang, H. H.; Ni, Z. H. Synthesis and Drug Release Properties of Poly(ethylene oxide) Segmented Polysulfone Copolymers. *J. Controlled Release* **2008,** *127*, 267–272.
11. Puskas, J. E.; Munoz-Robledo, L. G.; Hoerr, R. A.; Foley, J.; Schmidt, S. P.; Evancho-Chapman, M.; Dong, J. P.; Frethem, C.; Haugstad, G. Drug-Eluting Stent Coatings. *Wiley Interdiscip. Rev.: Nanomed. Nanobiotechnol.* **2009,** *1*, 451–462.
12. Wu, M.; Kleiner, L.; Tang, F. W.; Hossainy, S.; Davies, M. C.; Roberts, C. J., Surface Characterization of Poly(lactic acid)/Everolimus and Poly(ethylene vinyl alcohol)/Everolimus Stents. *Drug Delivery 17*, 376-384.
13. Xu, L. C.; Siedlecki, C. A. Atomic Force Microscopy Studies of the Initial Interactions between Fibrinogen and Surfaces. *Langmuir* **2009,** *25*, 3675–3681.
14. George, P. A.; Donose, B. C.; Cooper-White, J. J. Self-Assembling Polystyrene-*block*-poly(ethylene oxide) Copolymer Surface Coatings: Resistance to Protein and Cell Adhesion. *Biomaterials* **2009,** *30*, 2449–2456.
15. Seo, J. H.; Matsuno, R.; Takai, M.; Ishihara, K. Cell Adhesion on Phase-Separated Surface of Block Copolymer Composed of Poly(2-methacryloyloxyethyl phosphorylcholine) and Poly(dimethylsiloxane). *Biomaterials* **2009,** *30*, 5330–5340.
16. Mao, X. L.; Peng, H.; Ling, J. Q.; Friis, T.; Whittaker, A. K.; Crawford, R.; Xiao, Y. Enhanced Human Bone Marrow Stromal Cell Affinity for Modified Poly(L-lactide) Surfaces by the Upregulation of Adhesion Molecular Genes. *Biomaterials* **2009,** *30*, 6903–6911.
17. Fasolka, M. J.; Mayes, A. M. Block Copolymer Thin Films: Physics and Applications. *Annu. Rev. Mater. Res.* **2001,** *31*, 323–355.
18. Fasolka, M. J.; Banerjee, P.; Mayes, A. M.; Pickett, G.; Balazs, A. C. Morphology of Ultrathin Supported Diblock Copolymer Films: Theory and Experiment. *Macromolecules* **2000,** *33*, 5702–5712.
19. Huang, E.; Russell, T. P.; Harrison, C.; Chaikin, P. M.; Register, R. A.; Hawker, C. J.; Mays, J. Using Surface Active Random Copolymers to Control the Domain Orientation in Diblock Copolymer Thin Films. *Macromolecules* **1998,** *31*, 7641–7650.
20. Pickett, G. T.; Balazs, A. C. Equilibrium Orientation of Confined Diblock Copolymer Films. *Macromolecules* **1997,** *30*, 3097–3103.
21. Tang, W. H. Confinement of Symmetric Diblock Copolymer Thin Films. *Macromolecules* **2000,** *33*, 1370–1384.
22. Geisinger, T.; Muller, M.; Binder, K. Symmetric Diblock Copolymers in Thin Films. II. Comparison of Profiles between Self-Consistent Field Calculations and Monte Carlo Simulations. *J. Chem. Phys.* **1999,** *111*, 5251–5258.
23. Wang, Q.; Yan, Q. L.; Nealey, P. F.; de Pablo, J. J. Monte Carlo Simulations of Diblock Copolymer Thin Films Confined between Two Homogeneous Surfaces. *J. Chem. Phys.* **2000,** *112*, 450–464.
24. Groot, R. D.; Madden, T. J. Dynamic Simulation of Diblock Copolymer Microphase Separation. *J. Chem. Phys.* **1998,** *108*, 8713–8724.
25. Huang, C. I.; Lin, Y. C. Hierarchical Structure-within-Structure Morphologies in A-block-(B-Graft-C) Molecules. *Macromol. Rapid Commun.* **2007,** *28*, 1634–1639.
26. Lee, W. J.; Ju, S. P.; Wang, Y. C.; Chang, J. G., Modeling of Polyethylene and Poly(L-lactide) Polymer Blends and Diblock Copolymer: Chain Length and Volume Fraction Effects on Structural Arrangement. *J. Chem. Phys.* 2007, *127*.
27. Li, X. J.; Guo, J. Y.; Liu, Y.; Liang, H. J., Microphase Separation of Diblock Copolymer Poly(styrene-*b*-isoprene): A Dissipative Particle Dynamics Simulation Study. *J. Chem. Phys.* 2009, *130*.
28. Schultz, A. J.; Hall, C. K.; Genzer, J. Computer Simulation of Copolymer Phase Behavior. *J. Chem. Phys.* **2002,** *117*, 10329–10338.
29. Murat, M.; Grest, G. S.; Kremer, K. Statics and Dynamics of Symmetric Diblock Copolymers: A Molecular Dynamics Study. *Macromolecules* **1999,** *32*, 595–609.
30. Rotella, C.; Napolitano, S.; De Cremer, L.; Koeckelberghs, G.; Wubbenhorst, M., Distribution of Segmental Mobility in Ultrathin Polymer Films. *Macromolecules 43*, 8686-8691.
31. Sommer, J. U.; Hoffmann, A.; Blumen, A. Block Copolymer Films between Neutral Walls: A Monte Carlo Study. *J. Chem. Phys.* **1999,** *111*, 3728–3732.
32. Pickett, G. T.; Witten, T. A.; Nagel, S. R. Equilibrium Surface Orientation of Lamellae. *Macromolecules* **1993,** *26*, 3194–3199.
33. Jones, R. L.; Kumar, S. K.; Ho, D. L.; Briber, R. M.; Russell, T. P. Chain Conformation in Ultrathin Polymer Films. *Nature* **1999,** *400*, 146–149.
34. Beaucage, G.; Banach, M. J.; Vaia, R. A. Relaxation of Polymer Thin Films in Isothermal Temperature-Jump Measurements. *J. Polym. Sci., Part B: Polym. Phys.* **2000,** *38*, 2929–2936.
35. Smith, A. P.; Douglas, J. F.; Meredtih, J. C.; Amis, E. J.; Karim, A., Combinatorial Study of Surface Pattern Formation in Thin Block Copolymer Films. *Phys. Rev. Lett.* 2001,
36. Smith, A. P.; Douglas, J. F.; Amis, E. J.; Karim, A. Effect of Temperature on the Morphology and Kinetics of Surface Pattern Formation in Thin Block Copolymer Films. *Langmuir* **2007,** *23*, 12380–12387.